Electronic Supplementary Material (ESI) for Nanoscale Advances.
This journal is © The Royal Society of Chemistry 2021

Supporting Information

# PEDOT:PSS-Glued $MoO_3$ Nanowires Network for All-Solid-State Flexible Transparent Supercapacitors

Jie Liang,[a] Hongwei Sheng,[a] Qi Wang,[a] Jiao Yuan,[a] Xuetao Zhang,[a] Qing Su,[a] Erqing Xie,[a] Wei Lan,[a,*] Chuanfang (John) Zhang[b*]

[a] Key Laboratory of Special Function Materials and Structure Design, Ministry of Education, School of Physical Science and Technology, Lanzhou University, Lanzhou, 730000, People's Republic of China

[b] Laboratory for Functional Polymers, Empa, Swiss Federal Laboratories for Materials Science and Technology, ETH Domain, Überlandstrasse 129, CH-8600, Dübendorf, Switzerland

* Corresponding author

E-mail: lanw@lzu.edu.cn (W. Lan), chuanfang.zhang@empa.ch (C. Zhang)

## Calculations

The areal capacitance of AgNFs/$MoO_3$/PEDOT:PSS (AMP) film electrodes and the assembled flexible transparent supercapacitors (FTSCs) was calculated from CV and GCD curves based on the following equations, respectively:

$$C = \frac{1}{2v\Delta V}\oint I(V)dV \tag{1}$$

$$C = \frac{I(A)\Delta t}{\Delta V} \tag{2}$$

$$Carea = \frac{C}{S} \tag{3}$$

where $C$ is a total capacitance in F, $v$ is a scan rate in V $s^{-1}$, $I$(V) is an instant current, and $V$ is an applied voltage in V. $I$(A) refers to the discharge current; $\Delta V$(V) represents the changed potential during the discharge time $\Delta t$(s), and $S$ corresponds to the effective area of AMP electrodes.

The energy density ($E$) and power density ($P$) of the FTSCs were calculated using the following equations:

$$E = \frac{1}{2} \times C\text{area} \times \frac{(\Delta V)^2}{3600} \tag{4}$$

$$P = \frac{E}{\Delta t} \times 3600 \tag{5}$$

Where $E$ and $P$ correspond to the areal energy density and power density, respectively.

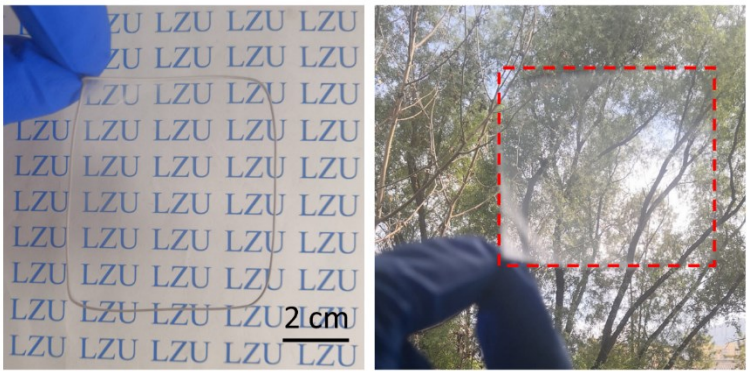


Fig. S1. Optical photographs of a freestanding AgNFs network.

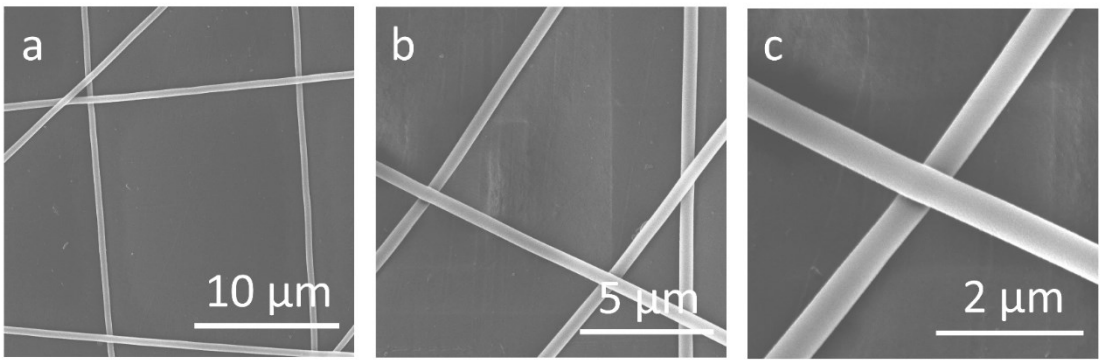


Fig. S2. SEM images of AgNFs network.

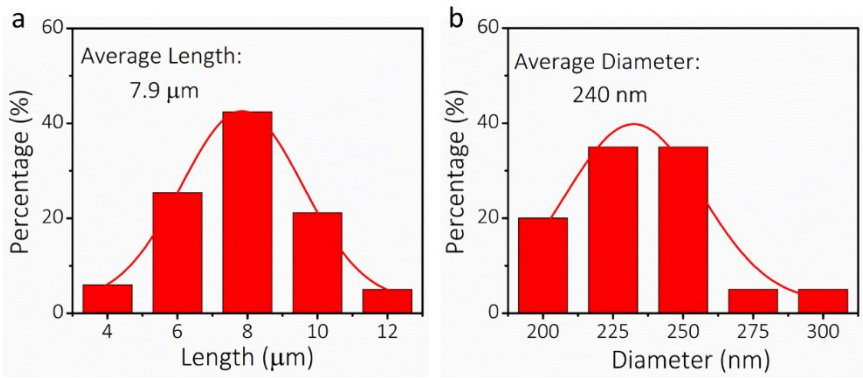


Fig. S3. (a) Length histogram and (b) diameter histogram of the as-synthesized $MoO_3$ nanowires.

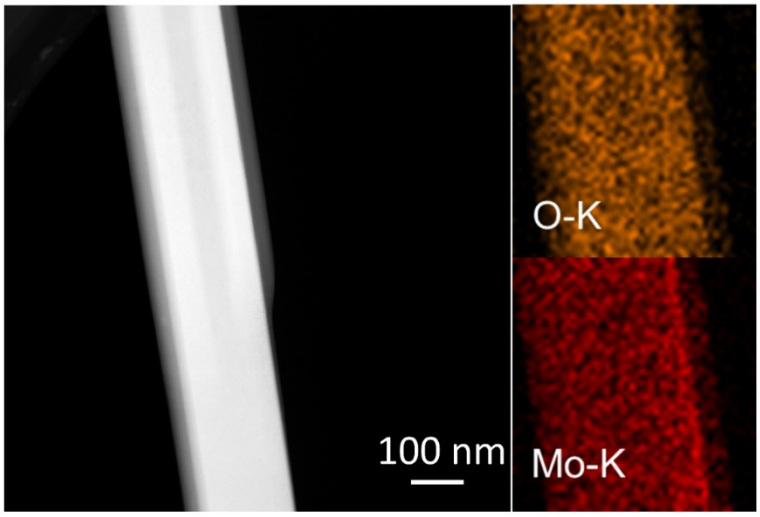


Fig. S4. Element mapping images of the as-synthesized $MoO_3$ nanowires.

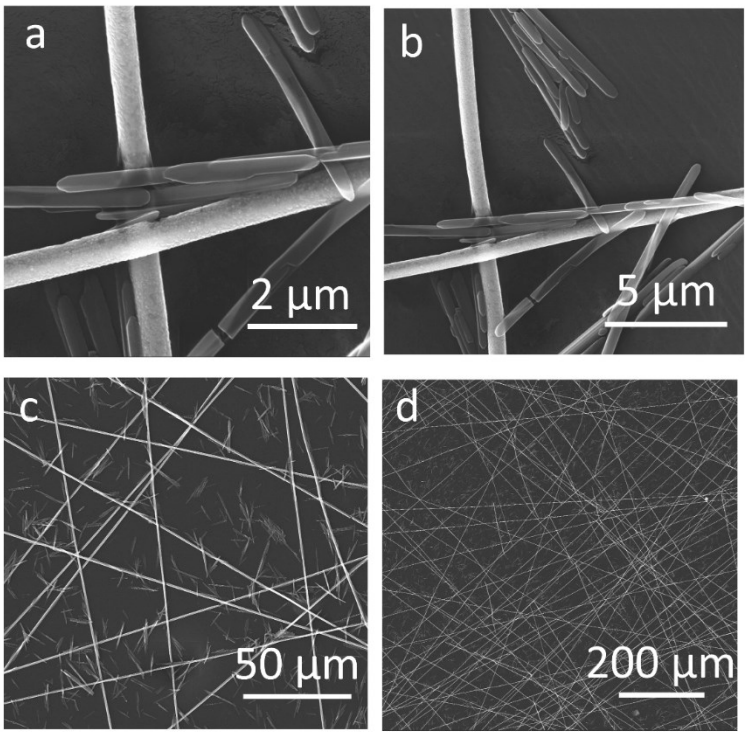


Fig. S5. SEM images of AMP electrode (the precursor ratio of 6:1).

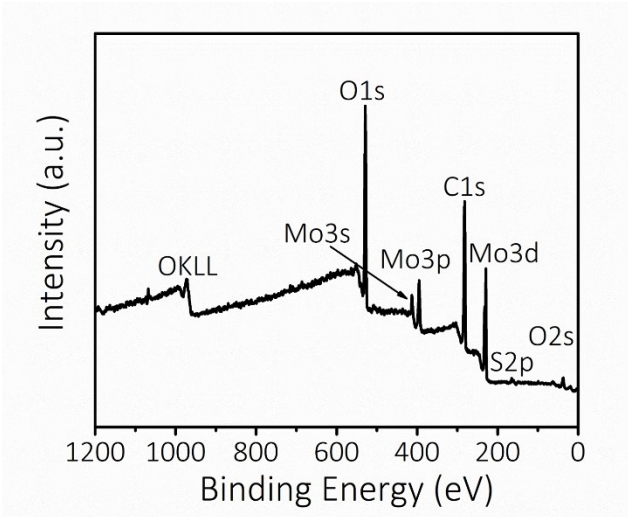


Fig. S6. XPS spectrum of PEDOT:PSS-glued $MoO_3$ nanowires (the precursor ratio of 6:1).

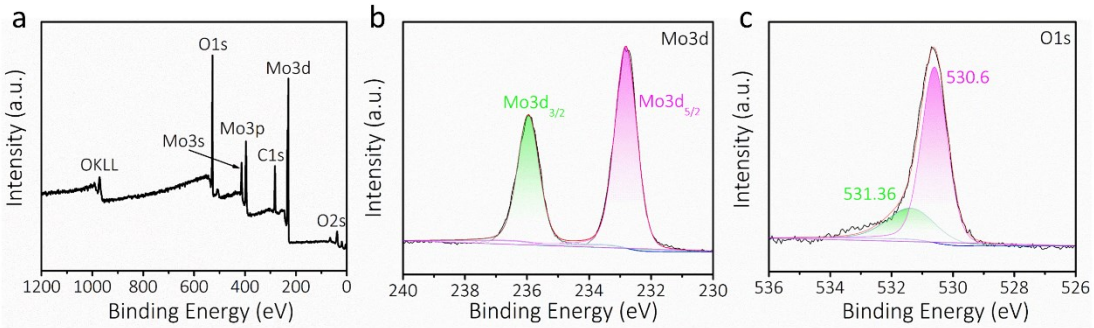


Fig. S7. (a) XPS survey spectrum of $MoO_3$ nanowires. High-resolution XPS spectra of (b) Mo 3d, and (c) O 1s for $MoO_3$ nanowires.

The survey spectrum (Fig. S7a) indicates the presence of Mo and O elements. The Mo $3d_{5/2}$ and Mo $3d_{3/2}$ peaks located at 232.8 and 235.9 eV reveal a +6 oxidation state of $MoO_3$ phase (Fig. S7b). The O1s peak at 530.6 eV (Fig. S7c) corresponds to the oxygen atoms of $MoO_3$, and the one centered at 531.4 eV is related to the adsorbed oxygen.

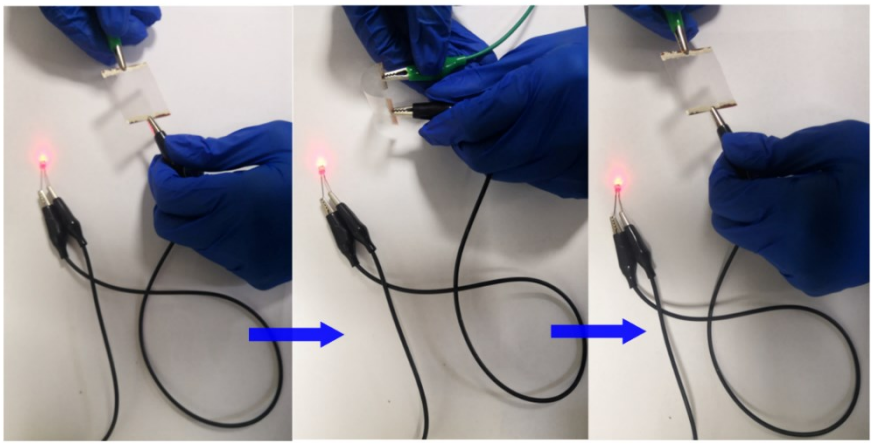

Fig. S8. Optical photographs of AgNFs network connected in a LED circuit.

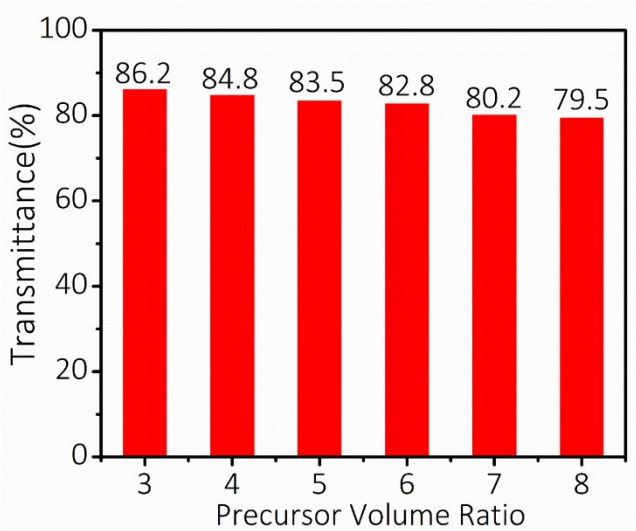


Fig. S9. The optical transmittances at 550 nm for the electrodes with different precursor ratios.

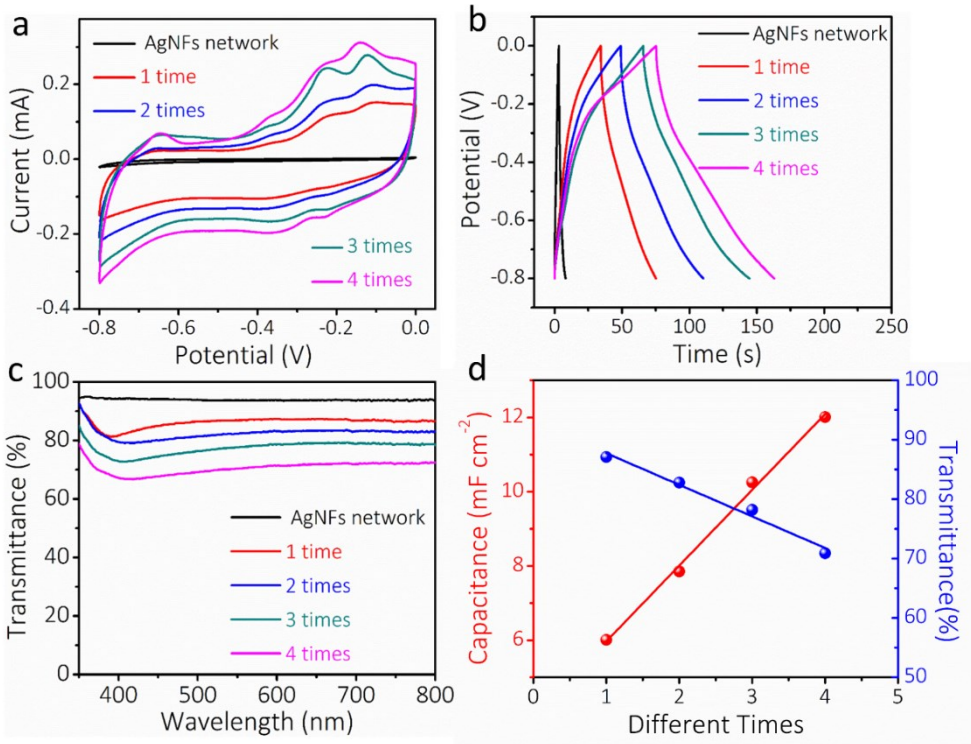


Fig. S10. Electrochemical performance of AMP electrodes (precursor ratio of 6:1) that were spin-coated the precursor hybrid dispersion for 1 to 4 times, AgNFs network was as a control experiment; (a) CV patterns at 10 mV $s^{-1}$, (b) GCD patterns at 0.10 mA $cm^{-2}$; (c) Transmittance spectra of AMP electrodes; (d) Optical transmittance and areal capacitance calculated by GCD curves.

Fig. S10a presents CV curves measured at 10 mV $s^{-1}$ for AMP electrodes with different spin-coating times. The enclosed area of CV curves enlarges with increasing spin-coating times, indicating an enhanced areal capacitance. Fig. S10b shows GCD curves at a current density of 0.10 mA $cm^{-2}$, the charge-discharge time of AMP electrodes is increased sequentially. The CV and GCD curves indicate that the electrochemical performance becomes better with the increase of spin-coating times. Meanwhile, the optical transparency of film electrodes is gradually degradable due to the more $MoO_3$ nanowires in the film electrodes (Fig. S10c). The calculated areal capacitance and optical transmittance at 550 nm are collected in Fig. S10d. The linear relationship is found with the spin-coating times of AMP precursor hybrid dispersion. For each spin-coating time, the areal capacitance of 1.56 mF $cm^{-2}$ is enhanced, and the

optical transmittance of 5.32 % is degraded.

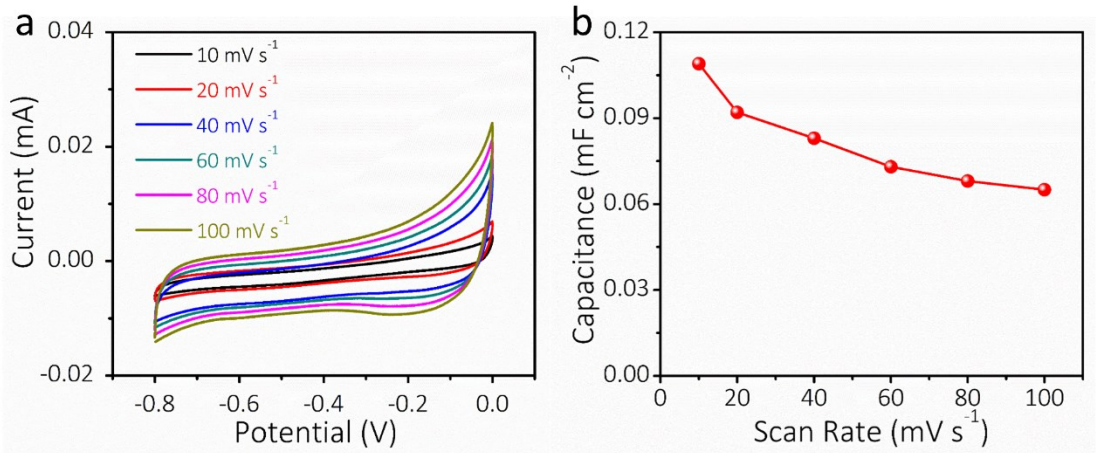


Fig. S11. (a) CV curves at different scan rates for the AgNFs network, and (b) the areal capacitance as a function of scan rate determined from the CV curves.

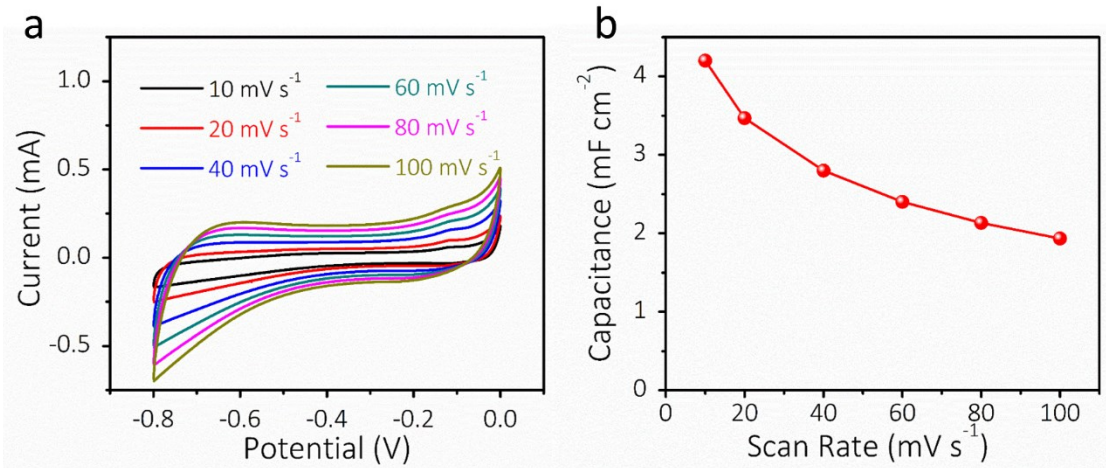


Fig. S12. (a) CV curves at different scan rates for the AgNFs/$MoO_3$ (AM) electrodes, and (b) the areal capacitance as a function of scan rate determined from the CV curves.

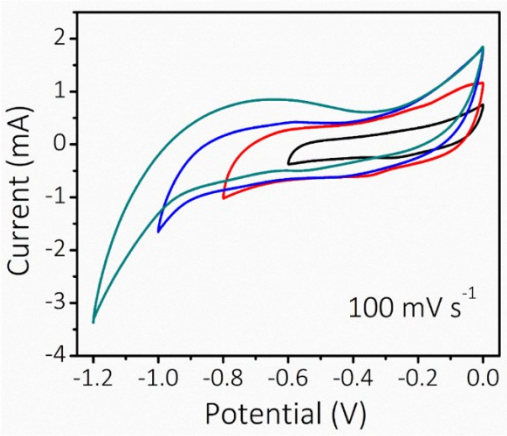


Fig. S13. CV curves measured at 100 mV $s^{-1}$ for AMP electrode (precursor ratio of 6:1) with different voltage windows.

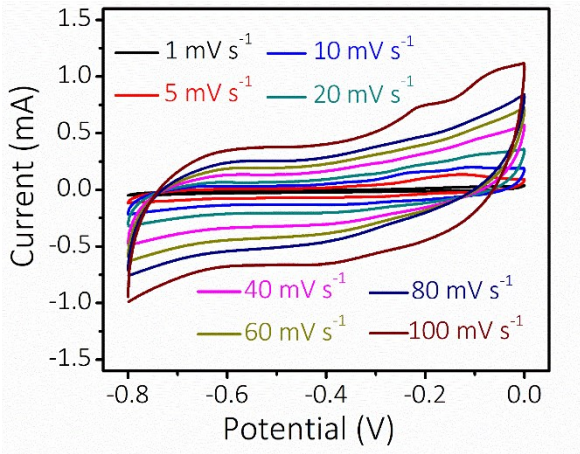


Fig. S14. CV curves at different scan rates for AMP electrodes (precursor ratio of 6:1).

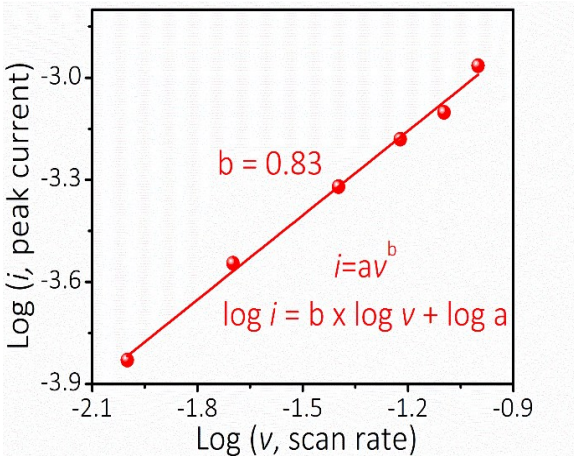


Fig. S15. The current response against scan rate and the extracted b-value for AMP electrodes (precursor ratio of 6:1).

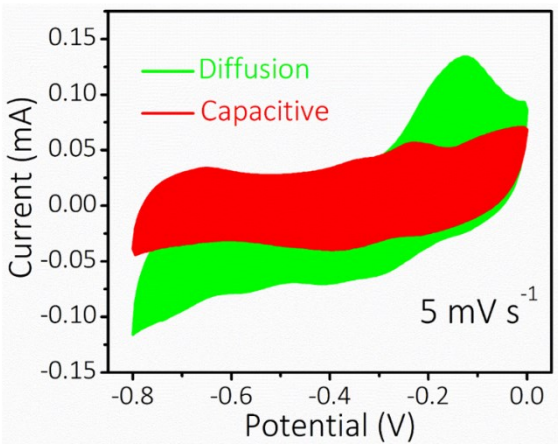


Fig. S16. The capacitive contribution in CV results of AMP electrode (precursor ratio of 6:1) at 5 mV $s^{-1}$.

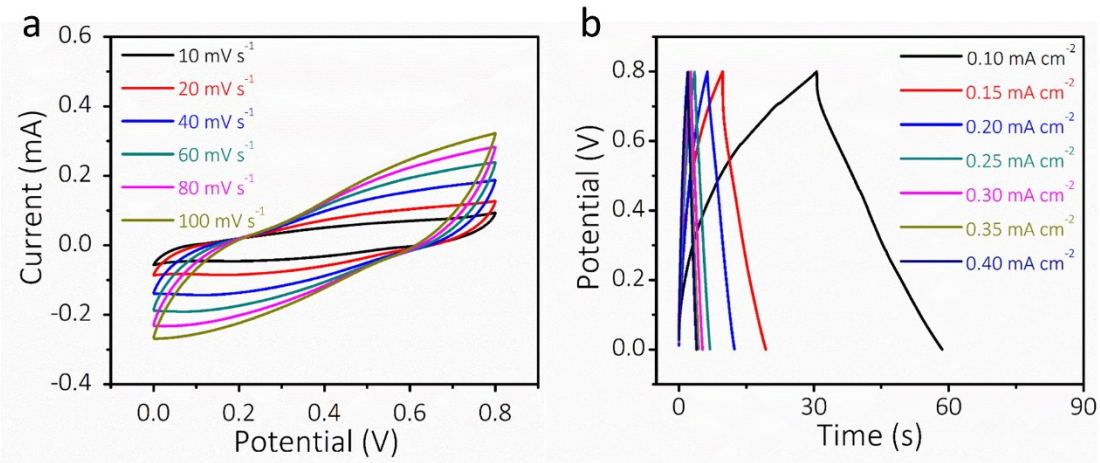


Fig. S17. CV curves at different scan rates and GCD curves at different current densities for the AM-based FTSC devices.

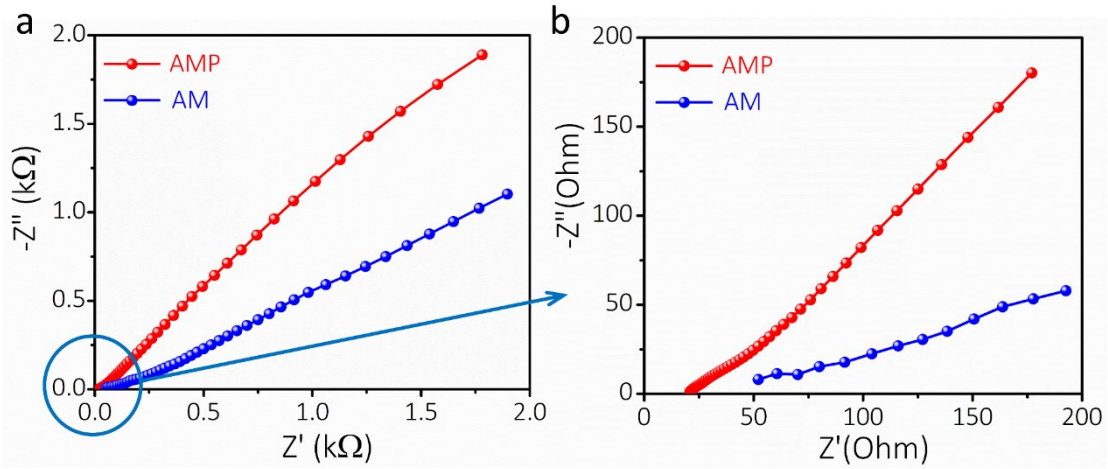

Fig. S18. EIS curves of (a) the AMP-based and (b) AM-based FTSC devices.

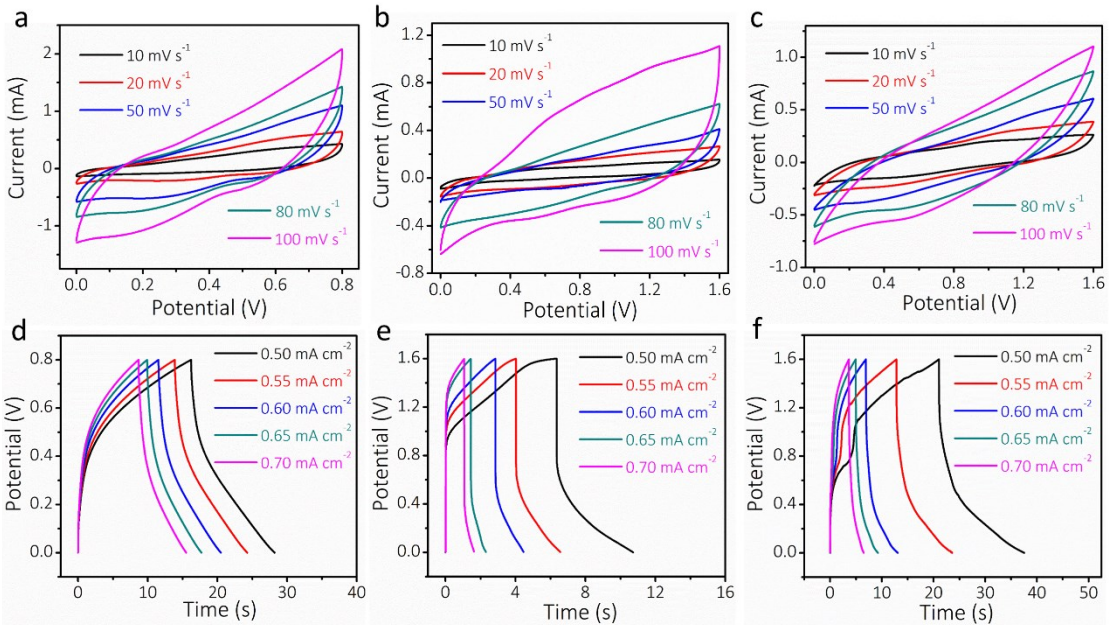


Fig. S19. CV curves of two FTSCs connected in parallel (a), in series (b), and two ones in series with the one in parallel (c). GCD curves of two FTSCs connected in parallel (d), in series (e), and two ones in series with the one in parallel (f).

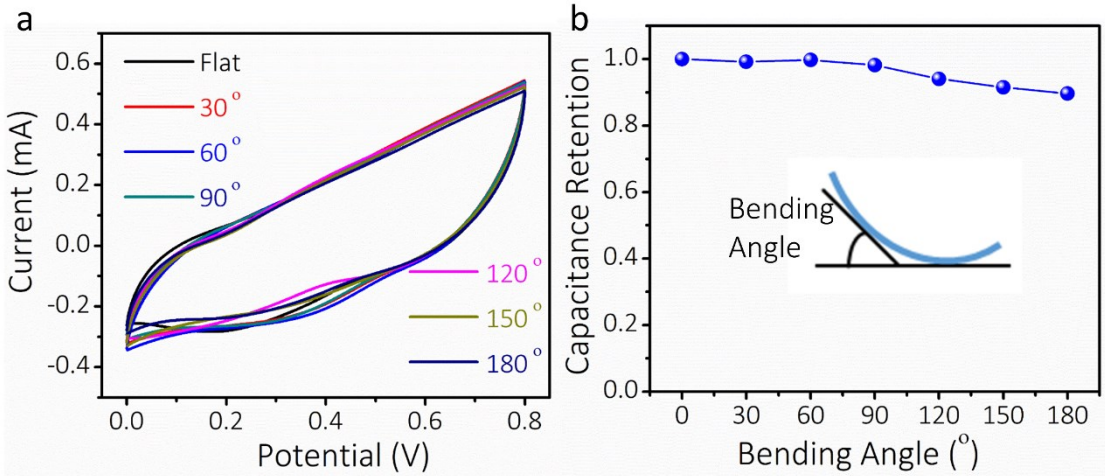


Fig. S20. The electrochemical performance of AMP-based FTSCs under different bending angles. (a) CV curves at 50 mV $s^{-1}$ and (b) the calculated capacitance retention.

Table S1. Comparison of the sheet resistance, optical transparency, and mechanical flexibility of transparent electrodes after 1000 bending cycles.

| Material | Rs ($\Omega$ $sq^{-1}$) | Transmittance (T %) | $R/R_0$ | Bending radius (mm) | Reference |
|---|---|---|---|---|---|
| Cu nanofibers | 50 | 90 | 1.1 | -- | [1] |
| AgNWs/PEDOT:PSS | 45 | 92 | 1.2 | -- | [2] |
| Ag grid | 30 | 85 | 1.03 | 15 | [3] |
| Ag grid | 6.8 | 82 | 1.3 | 10 | [4] |
| Ag grid | 5.2 | 91 | 1.6 | 15 | [5] |
| AgNFs/$MoO_3$ /PEDOT:PSS | 9.7 | 82.8 | 1.05 | 10 | This work |

Table S2. Comparison of the areal capacitance and optical transparency for transparent supercapacitors.

| Material | Capacitance (mF $cm^{-2}$) | Transmittance (T %) | Reference |
|---|---|---|---|
| PEDOT:PSS | 1.18 | 65 | [6] |
| Graphene | 3.3 | 47 | [7] |
| $RuO_2$/PEDOT | 0.84 | 80 | [8] |
| PEDOT:PSS/AgNWs | 0.6 | 51 | [9] |
| $MnO_2$/ITO/PET | 4.73 | 44 | [10] |
| $MnO_2$@AuNFs | 2.07 | 79 | [11] |
| $Co(OH)_2$ /AgNWs | 0.54 | 54 | [12] |
| Au@$MnO_2$ nanomesh | 0.795 | 36 | [13] |
| HTSE film | 3.64 | 85 | [14] |
| GNHC-GF | 5.48 | 44 | [15] |
| AgNFs/$MoO_3$ /PEDOT:PSS | 6.33 | 65 | This work |

Table S3. Energy densities and power densities of our FTSCs device in comparison with the reported transparent supercapacitors.

| Active material | Power density (μW $cm^{-2}$) | Energy density (μWh $cm^{-2}$) | Reference |
|---|---|---|---|
| $Ti_3C_2Tx$ (symmetric) | 0.62 | 0.049 | [16] |
| | 1.24 | 0.034 | |
| | 2.51 | 0.025 | |
| | 5.14 | 0.02 | |
| | 10.91 | 0.018 | |
| PEDOT:PSS | 1.16 | 0.009 | [17] |
| | 1.82 | 0.008 | |
| | 3.7 | 0.008 | |
| | 11.76 | 0.0079 | |
| | 20.92 | 0.006 | |
| $RuO_2$/PEDOT:PSS | 0.28 | 0.015 | [8] |
| | 1.13 | 0.014 | |
| | 2.08 | 0.014 | |
| | 4.83 | 0.014 | |
| | 19.47 | 0.011 | |
| Graphene QDs | 0.094 | 0.00079 | [18] |
| | 0.083 | 0.00082 | |
| | 0.072 | 0.00084 | |
| | 0.062 | 0.00087 | |
| RMGO | 9 | 0.014 | [19] |
| CVD-Graphene | 2 | 0.0028 | [19] |
| AgNFs/$MoO_3$ /PEDOT:PSS | 40 | 0.623 | This work |
| | 60 | 0.538 | |
| | 80 | 0.459 | |
| | 100 | 0.400 | |

| | |
|---|---|
| 120 | 0.342 |
| 140 | 0.302 |
| 160 | 0.282 |

## Notes and references


1. H. Wu, L. Hu, M. W. Rowell, D. Kong, J. J. Cha, J. R. McDonough, J. Zhu, Y. Yang, M. D. McGehee and Y. Cui, *Nano Lett.*, 2010, **10**, 4242-4248.
2. R. T. Ginting, M. M. Ovhal and J. W. Kang, *Nano Energy*, 2018, **53**, 650-657.
3. S. Hong, J. Yeo, G. Kim, D. Kim, H. Lee, J. Kwon, H. Lee, P. Lee and S. H. Ko, *ACS Nano*, 2013, **7**, 5024-5031.
4. Y. Lee, W. Y. Jin, K. Y. Cho, J. W. Kang and J. Kim, *J. Mater. Chem. C*, 2016, **4**, 7577-7583.
5. Y. S. Oh, D. Y. Choi and H. J. Sung, *RSC Adv.*, 2015, **5**, 64661-64668.
6. T. Cheng, Y. Z. Zhang, J. P. Yi, L. Yang, J. D. Zhang, W. Y. Lai and W. Huang, *J. Mater. Chem. A*, 2016, **4**, 13754-13763.
7. N. Li, G. Yang, Y. Sun, H. Song, H. Cui, G. Yang and C. Wang, *Nano Lett.*, 2015, **15**, 3195-3203.
8. C. F. Zhang, T. M. Higgins, S. H. Park, S. E. O'Brien, D. H. Long, J. Coleman and V. Nicolosi, *Nano Energy*, 2016, **28**, 495-505.
9. X. Liu, D. Li, X. Chen, W. Y. Lai and W. Huang, *ACS Appl. Mater. Interfaces*, 2018, **10**, 32536-32542.
10. Y. Wang, W. Zhou, Q. Kang, J. Chen, Y. Li, X. Feng, D. Wang, Y. Ma and W. Huang, *ACS Appl. Mater. Interfaces*, 2018, **10**, 27001-27008.
11. S. B. Singh, T. I. Singh, N. H. Kim and J. H. Lee, *J. Mater. Chem. A*, 2019, **7**, 10672-10683.
12. H. Sheng, X. Zhang, Y. Ma, P. Wang, J. Zhou, Q. Su, W. Lan, E. Xie and C. J.

Zhang, *ACS Appl. Mater. Interfaces*, 2019, **11**, 8992-9001.

13. T. Qiu, B. Luo, M. Giersig, E. M. Akinoglu, L. Hao, X. Wang, L. Shi, M. Jin and L. Zhi, *Small*, 2014, **10**, 4136-4141.

14. S. B. Singh, T. Kshetri, T. I. Singh, N. H. Kim and J. H. Lee, *Chem. Eng. J.*, 2019, **359**, 197-207.

15. N. Li, X. Huang, H. Zhang, Z. Shi and C. Wang, *J. Mater. Chem. A*, 2017, **5**, 16803-16811.

16. C. J. Zhang, B. Anasori, A. Seral-Ascaso, S. H. Park, N. McEvoy, A. Shmeliov, G. S. Duesberg, J. N. Coleman, Y. Gogotsi and V. Nicolosi, *Adv. Mater.*, 2017, **29**, 1702678.

17. T. M. Higgins and J. N. Coleman, *ACS Appl. Mater. Interfaces*, 2015, **7**, 16495-16506.

18. K. Lee, H. Lee, Y. Shin, Y. Yoon, D. Kim and H. Lee, *Nano Energy*, 2016, **26**, 746-754.

19. J. J. Yoo, K. Balakrishnan, J. Huang, V. Meunier, B. G. Sumpter, A. Srivastava, M. Conway, A. L. Reddy, J. Yu, R. Vajtai and P. M. Ajayan, *Nano Lett.*, 2011, **11**, 1423-1427.